PERGAMON

International Journal of Plasticity 18 (2002) 1373–1393

INTERNATIONAL JOURNAL OF Plasticity

www.elsevier.com/locate/ijplas

Modeling the evolution of anisotropy in Al–Li alloys: application to Al–Li 2090-T8E41

H. Garmestani[a,*], S.R. Kalidindi[b], L. Williams[a], C.M. Bacaltchuk[a], C. Fountain[a], E.W. Lee[c], O.S. Es-Said[d]

[a]*FAMU-FSU College of Engineering, Department of Mechanical Engineering and Center for Materials Research and Technology (MARTECH), Tallahassee, FL 32310-6046, USA*

[b]*Department of Materials Engineering, Drexel University, Philadelphia, PA 19104, USA*

[c]*Code 4342, M55, Bldg 2188, Naval Air Systems Command, Patuxent River, MD 20670, USA*

[d]*Department of Mechanical Engineering, Loyola Marymount University, Los Angeles, CA 90045-8145, USA*

Received in final revised form 21 September 2001

Abstract

It is widely reported in current literature that the precipitation hardened Al–Li sheet alloys exhibit extremely high anisotropy in yield (and ultimate tensile) strength, which is well beyond what can be explained as purely a consequence of the strong crystallographic texture in the material (e.g. J. Mater. Sci. Eng. A265, 1999, 100). This paper presents a crystal plasticity based modeling framework that will (i) facilitate the segregation of the contributions to the overall anisotropy from crystallographic texture and precipitation hardening, and (ii) correlate the contribution from precipitate hardening to either co-planar slip activity or the non-coplanar slip activity in the cold-working step prior to the aging heat treatment. More specifically, a Taylor-type (fully-constrained) crystal plasticity model was formulated to predict the yield strength of the fully processed sheet and its anisotropy, while accounting for the initial texture in the hot-worked sheet, its evolution during the cold-working step prior to aging, and the inhomogeneous nucleation of the T_1 phase platelets (these are known to form on {111} planes, but not usually in equal amounts on the different {111} planes in a given crystal). In an effort to illustrate the methodology developed in the study, a limited set of experiments was conducted on Al–Li 2090-T8E41 alloy sheet. Off-axis stretches were applied on the sheet at room temperature prior to the aging treatment, and the mechanical anisotropy in the fully processed sheets was characterized by performing tension tests on coupons cut from the sheet at 0, 30, 45, 60 and 90° to the original rolling direction (RD). Both the initial texture in the sheet and its evolution during the different off-axis stretches were characterized. The alloys

* Corresponding author. Tel.: +1-850-644-5993; fax: +1-850-644-9281.
E-mail address: garm@magnet.fsu.edu (H. Garmestani).

PII: S0749-6419(01)00073-0

processed in this study showed pronounced anisotropy. The application of the methodology developed in this study revealed that much of the observed anisotropy in this particular data set could be explained by accounting for the texture in the sample in the processed condition. Although the data set available was inadequate to establish clear correlations of the anisotropy with preferential hardening mechanisms arising from either co-planar or non-co-planar slip activity during the off-axis stretch, there were indications favoring the latter. This case study, however, illustrates the application of the methodology developed in this study to obtain better insight into the nature of the anisotropy in these sheets and its physical origin.

Keywords: A. Precipitation hardening; A. Crystallographic texture; B. Anisotropic material; C. Cross rolling; C. Crystal plasticity

1. Introduction

In recent years, Al–Li alloys have received considerable attention because of their high modulus, specific strength and low density. These properties are particularly attractive to designers of high performance military and commercial aircraft. Aluminum–lithium alloys processed through ingot metallurgy (IM) casting with subsequent forming operations are being currently developed for aerospace applications (Kim et al., 2000; Miller et al., 1986; Yoon et al., 2000). However, commercial Al–Li alloys exhibit significant tensile strength anisotropy when compared to conventional 2xxx and 7xxx type aerospace alloys (Es-Said and Lee, 1995; Flower and Gregson, 1987; Lucke et al., 1986).

While the microstructures and mechanical properties of IM aluminum alloys processed under different conditions have been characterized extensively, the correlations between the microstructure and properties are still a subject of current research (Lee et al., 1999). Thermomechanical treatments such as rolling and stretching have been employed to improve the overall mechanical properties of these alloys (Li, 2000; Trinca et al., 2000; Lee et al., 1999). Using these techniques, highly textured sheet metals with pronounced mechanical anisotropy are produced, which may not be desirable for some industrial applications (Es-Said et al., 1995). It is generally recognized that crystallographic texture plays an important role in the mechanical anisotropy exhibited by these sheets (Miller et al., 1986; Lee et al., 1999; Inal, 2000; Ceccaldi, 1994; Peeters et al., 2001).

T_1 (Al_2CuLi) precipitate is the major source of strengthening in Al–Li–Cu alloys (Kim and Lee, 1993). This precipitate has a hexagonal structure, and occurs as thin plates on {111} planes, which also happen to be the slip planes for face-centered cubic alloys. In a TEM study, Kim and Lee (1993) have shown that there is an inhomogeneous distribution of T_1 precipitates among the four {111} habit planes after stretching and aging of a 2090 Al–Li alloy. Their observations suggest that a higher density of the T_1 precipitates are produced on the specific slip planes that experienced a higher slip activity. It was further reported that this inhomogeneous distribution of T_1 precipitates has a direct effect on the mechanical anisotropy of the

material. More recently, Es-Said and Lee (1995) and Lee et al. (1999) have reported success in reducing mechanical anisotropy of 2095 Al–Li sheets by the incorporation of off-axis rolling/stretching prior to aging.

It is clear from the above discussion that the reported anisotropy in Al–Li alloys can be attributed to at least two factors: (i) the strong texture in these alloys in the processed condition, and (ii) the inhomogeneous nucleation of T_1 precipitates. The precise contributions from these two factors are not clearly known at the present time. It is quite difficult to assess the contribution to the overall anisotropy from the second factor listed above (Lee and Frazier, 1988; Chandler and Gortzen, 1994; Peters et al., 1986; Kim and Lee, 1993; Yao et al., 1991; Vasudevan et al., 1988). Most of the past work in this area has focused on correlating properties with precipitate size or spacing (Tsao et al., 1999). Modeling of aging process only considers the thermodynamical features of the processing micromechanics (Kaneko and Oyamada, 2000). Other modeling attempts are based on the phenomenological aspect of the process using internal state variables representing anisotropy and internal stresses (Garmestani et al., 2001). A better understanding of this process requires integrated experimental and modeling efforts that attempt to relate crystallographic texture, anisotropy, and the inhomogeneous distribution of precipitates. Although it is relatively straightforward to carry out experimental investigations to characterize the mechanical anisotropy in the processed Al–Li sheets, establishing the relative contributions to these from the various micromechanisms involved is quite complex. Establishing these correlations from a purely experimental approach requires a prohibitively large number of investigations on transmission electron microscope. It is therefore desirable to obtain some clues from theory. In general, modeling theories are constructed to predict properties resulting from assumed constitutive behavior (Choi et al., 2000, Gall and Sehitoglu, 1999; Khan and Cheng, 1998; Barlat et al., 1997; Lin and Havner, 1994). They are, however, not readily amenable to identifying the correct constitutive behavior given a sufficiently large experimental database of the overall properties. For the present problem, the later approach is needed to guide further studies in this important research area.

The main objective of this study was to develop a suitable methodology that will facilitate the segregation of the respective contributions of the different factors described above to the overall anisotropy in the Al–Li alloys. For this purpose, we have developed a suitable framework that allows one to decouple the contributions to the anisotropy from texture and from hardening due to inhomogeneous precipitation, and to establish correlations of the latter with either co-planar or non-coplanar slip activity in the cold-working stage prior to the aging heat treatment. Application of the methodology requires the use of quantitative information on the texture in the material. Since such information was not readily available from previously reported studies in literature, it was necessary to conduct a new set of experiments to illustrate the methodology developed in this study. In the following, we first present the theoretical development of the methodology. Next, the application of the methodology is illustrated with a limited set of experiments on Al–Li 2090-T8E41 alloy sheets.

2. Development of the theoretical framework

2.1. Taylor-type crystal plasticity model

The most widely used modeling tool to account physically for the influence of underlying texture on the anisotropic yield strength of a given material is the Taylor model (Taylor, 1938) in its extended form (Asaro and Needleman, 1985). In this model it is assumed that all of the individual grains (or crystals) in the polycrystal possess the same volume and that they experience the same deformation gradient history. As a consequence of this simplifying assumption, the Taylor averaging procedure for estimating the response of the polycrystal often violates equilibrium between the individual grains and leads to an upper-bound estimate for the overall strength of the polycrystal. It has been shown that in spite of this limitation, the Taylor-type model produces fairly accurate predictions of the anisotropic yield strength of the material (Kalidindi and Schoenfeld, 2000). Furthermore, it is now well established that the Taylor-type model not only captures well the initial anisotropy of yield strength in the given material, but also predicts well the evolution of both the anisotropic stress-strain response and the averaged texture to large plastic strains for the single-phase, medium to high stacking fault energy, cubic, polycrystalline metals (Kalidindi et al., 1992; Bronkhorst et al., 1992).

The basic features of the Taylor-type model are presented first briefly. The reader is referred to earlier papers (Kalidindi et al., 1992) for further details of the model and the associated numerical procedures.

For a single crystal material undergoing finite deformations, we start with a multiplicative decomposition of the total deformation gradient (**F**) into elastic and plastic components as (Asaro and Needleman, 1985)

$$\mathbf{F} = \mathbf{F}^{*}\mathbf{F}^{\mathrm{p}} \tag{1}$$

F* contains deformation gradients due to both elastic stretching as well as the lattice rotation, while $\mathbf{F}^{\mathrm{p}}$ denotes the deformation gradient due to plastic deformation alone. The constitutive equation for stress in the crystal can be expressed as

$$\mathbf{T}^{*} = \mathbf{L}[\mathbf{E}^{*}], \qquad \mathbf{T}^{*} = (\det\mathbf{F}^{*})\mathbf{F}^{*-1}\mathbf{T}\mathbf{F}^{*-\mathrm{T}}, \qquad \mathbf{E}^{*} = \frac{1}{2}\left\{\mathbf{F}^{*\mathrm{T}}\mathbf{F}^{*} - \mathbf{1}\right\}, \tag{2}$$

where **L** is the fourth-order elasticity tensor, **T*** and **E*** are a pair of work conjugate stress and strain measures, and **T** is the Cauchy stress in the crystal. The evolution of $\mathbf{F}^{\mathrm{p}}$ can be expressed in a rate form as

$$\dot{\mathbf{F}}^{\mathrm{p}} = \mathbf{L}^{\mathrm{p}}\mathbf{F}^{\mathrm{p}}, \qquad \mathbf{L}^{\mathrm{p}} = \sum_{\alpha}\dot{\gamma}^{\alpha}\mathbf{S}_{\mathrm{o}}^{\alpha}, \qquad \mathbf{S}_{\mathrm{o}}^{\alpha} = \mathbf{m}_{\mathrm{o}}^{\alpha} \otimes \mathbf{n}_{\mathrm{o}}^{\alpha}, \tag{3}$$

where $\dot{\gamma}^{\alpha}$ is the shearing rate on the slip system α, and $\mathbf{m}_{\mathrm{o}}^{\alpha}$ and $\mathbf{n}_{\mathrm{o}}^{\alpha}$ denote the slip direction and the slip plane normal of the slip system, respectively, in the initial

unloaded configuration (Kalidindi et al., 1992). The shearing rate on the slip system is dependent on the resolved shear stress (τ^{α}) on the slip system and the slip resistance (s^{α}) of that slip system, and can be expressed in a power-law relationship as (Asaro and Needleman, 1985)

$$\dot{\gamma}^{\alpha} = \dot{\gamma}_{\mathrm{o}} \left| \frac{\tau^{\alpha}}{\mathrm{s}^{\alpha}} \right|^{1/\mathrm{m}} \mathrm{sgn}(\tau^{\alpha}), \qquad \tau^{\alpha} \approx \mathbf{T}^{*}\mathbf{S}_{\mathrm{o}}^{\alpha}, \tag{4}$$

where $\dot{\gamma}_{\mathrm{o}}$ denotes a reference value of the slip rate and m represents the strain rate sensitivity parameter. In the present study, $\dot{\gamma}_{\mathrm{o}}$ is taken as 0.001 s^{-1} and m is taken as 0.01, as is done routinely in literature for fcc polycrystals deformed at low homologous temperatures (see e.g. Kalidindi et al., 1992). In general, the evolution of the slip system resistance can be expressed as

$$\dot{\mathrm{s}}^{\alpha} = \sum_{\beta} h^{\alpha\beta} \left| \dot{\gamma}^{\beta} \right| \tag{5}$$

where $\mathrm{h}^{\alpha\beta}$ represent the slip hardening rates.

As described earlier, the most widely used approach to obtain the response of a polycrystal from the response of the individual grains is to use the extended Taylor's assumption of iso-deformation gradient in all of the crystals comprising the polycrystal. Furthermore, if all grains are assumed to be of the same size, the Cauchy stress in the polycrystal can be taken as a simple number average of the Cauchy stresses in the various grains. Therefore, employing Taylor's assumptions, the macroscopic Cauchy stress in the polycrystal can be expressed as

$$\bar{\mathbf{T}} = \frac{1}{N} \sum_{\mathrm{k}=1}^{N} \mathbf{T}^{(k)} \tag{6}$$

where N is the number of crystals in the aggregate, and $\mathbf{T}^{(\mathrm{k})}$ is the Cauchy stress in the crystal [labeled (k)].

2.2. Modeling the anisotropy of precipitation-hardened Al–Li alloys

The typical processing steps involved in processing of Al–Li alloy sheets are as follows. The hot-rolled sheet is solution treated and subjected to a small amount of cold-work (either by stretching or cold-rolling; Kim and Lee, 1993) in an effort to reduce the mechanical anisotropy in the sheet. The sheet is then aged to produce the precipitation hardening effect. In modeling the anisotropy resulting from these processes, in the present study, we start with a measured texture of the hot rolled sheet. It has been demonstrated in literature that the solution heat treatment step does not influence the texture in the material (Lee et al., 1999). It is therefore assumed that the texture is the same even after the solution heat treatment step.

The cold-working step (stretching or rolling) causes a change in texture as well as slip resistances on various slip systems, and these in turn can affect significantly the yield strength of the sheet and its anisotropy. The Taylor-type model described above can handle readily the microstructure evolution during the cold-working stage. The same model can also handle the changes in slip resistances during this step provided a suitable description of the slip hardening functions [expressions for $h^{\alpha\beta}$ in Eq. (5)] is available. However, these changes in slip resistances caused by slip activity in the cold-working step are expected to be relatively small compared to the changes caused in the aging step. Therefore, in the present study these are ignored (or alternatively assume to be combined with the treatment for changes caused by the aging treatment).

As described earlier, an important consideration in the present study is that the differences in slip activity on the various slip systems during the cold-working stage can lead to significant differences in slip resistances after being subjected to the aging heat treatment. This is because the T_1 precipitates that are produced during the aging heat treatment are assumed to form heterogeneously on the different {111} slip planes, in proportion to the slip activity on the respective planes (Kim and Lee, 1993; Lee et al., 1999). Note that this notion is consistent with the established concept that higher dislocation density promotes precipitate nucleation. However, the precise consequence of the higher incidence of the T_1 precipitates on certain {111} planes in the crystal on the slip hardening of the different slip systems in the crystal is not yet fully understood.

Due to the high symmetry of the fcc crystal structure and the presence of a single family of slip systems, it is convenient to classify the mechanism leading to differential hardening of slip systems as one that arises due to either the co-planar component of the slip activity or the non-co-planar component of slip activity during the cold working step prior to the aging step. It is implicitly assumed that the slip activity during the cold-working stage produces a heterogeneous distribution of the T_1 precipitates, which then leads to one of the two preferential hardening modes described above. It should be noted that this classification covers all possible phenomenology of slip hardening in this simple (and highly symmetric) class of materials. In the event that one of these components does not dominate (i.e. both co-planar slip activity and non-co-planar slip activity contribute equally to slip hardening as a net result of cold working and subsequent aging treatment) then the slip resistances of all slip systems would increase more or less equally, with no significant contribution to the anisotropy of the yield strength in the processed sheet. Therefore, the consequence of the differences in slip activity during the cold-working stage on the corresponding slip resistances in the aged condition (through inhomogeneous distribution of T_1 precipitates) can be studied by invoking one of the two following forms:

$$s^{\alpha} = s_{\mathrm{o}} + K^{\mathrm{cp}} \sum_{\substack{\beta \in \text{co-planar} \\ \text{slip systems of} \alpha}} \left|\gamma^{\beta}\right| \tag{7}$$

$$s^{\alpha} = s_{o} + K^{ncp} \sum_{\substack{\beta \in \text{non-coplanar} \\ \text{slip systems of} \alpha}} \left|\gamma^{\beta}\right| \tag{8}$$

where s_o represents a constant value for all slip systems (including the contributions from homogenous nucleation of precipitates other than T_1, if relevant), and K^{cp} and K^{ncp} represent modeling parameters. Note that Eq. (7) is suitable for situations where the co-planar slip activity causes preferential slip hardening, while Eq. (8) is suitable to model situations where the non-co-planar slip activity causes the preferential slip hardening process. In the present study, we develop a methodology to explore purely phenomenologically, if either of the functions described in Eqs. (7) and (8) can capture the anisotropy observed in the measurements.

The following specific procedure is suggested to separate the various contributions.

2.2.1. Step 1

The first objective should be to assess the direct contribution from texture itself. This is accomplished routinely in literature by computation of Taylor factors (Lee et al., 1999). Taylor factor is defined as the ratio of the yield strength in tension to the critical resolved shear stress (assumed to be same for all slip systems and all crystals). Starting with the measured texture in the hot rolled as-received sheet, one can simulate the cold-working step using the Taylor-type model described earlier (Kalidindi et al., 1992). This simulation provides a prediction of the texture in the sheet at the end of the cold-working step. Using this predicted texture, Taylor factors corresponding to different angles with respect to the rolling direction (on the plane of the sheet) can be computed, using the Taylor-type model and assuming that the slip resistances for all slip systems in all crystals are the same.

The experimental data characterizing the mechanical anisotropy of the sheet is often presented as off-axis yield strength (see e.g. Lee et al., 1999; or the experimental curves from the present study shown in Fig. 1). The measured off-axis yield strengths should be normalized by the corresponding computed Taylor factors. The motivation for this normalization is to examine what component of the measured anisotropy is attributable directly to texture. In other words, if texture was the only contributing factor to the yield strength anisotropy, then the normalized values of σ_y/M (σ_y being the yield strength and M being the Taylor factor for the specific texture) would not show any anisotropy (i.e. they would be constant as a function of the angle to the rolling direction).

2.2.2. Step 2

Next, we elucidate the contributions to the observed anisotropy from the preferential hardening of slip systems (due to inhomogeneous formation of T_1 precipitates). As described earlier, Eqs. (7) and (8) can be used to model the preferential hardening of slip systems due to co-planar slip activity and non-co-planar slip activity in the cold-working stage, respectively. The objective in this part of the study is to examine if either of these forms can explain the residual anisotropy after the step 1.

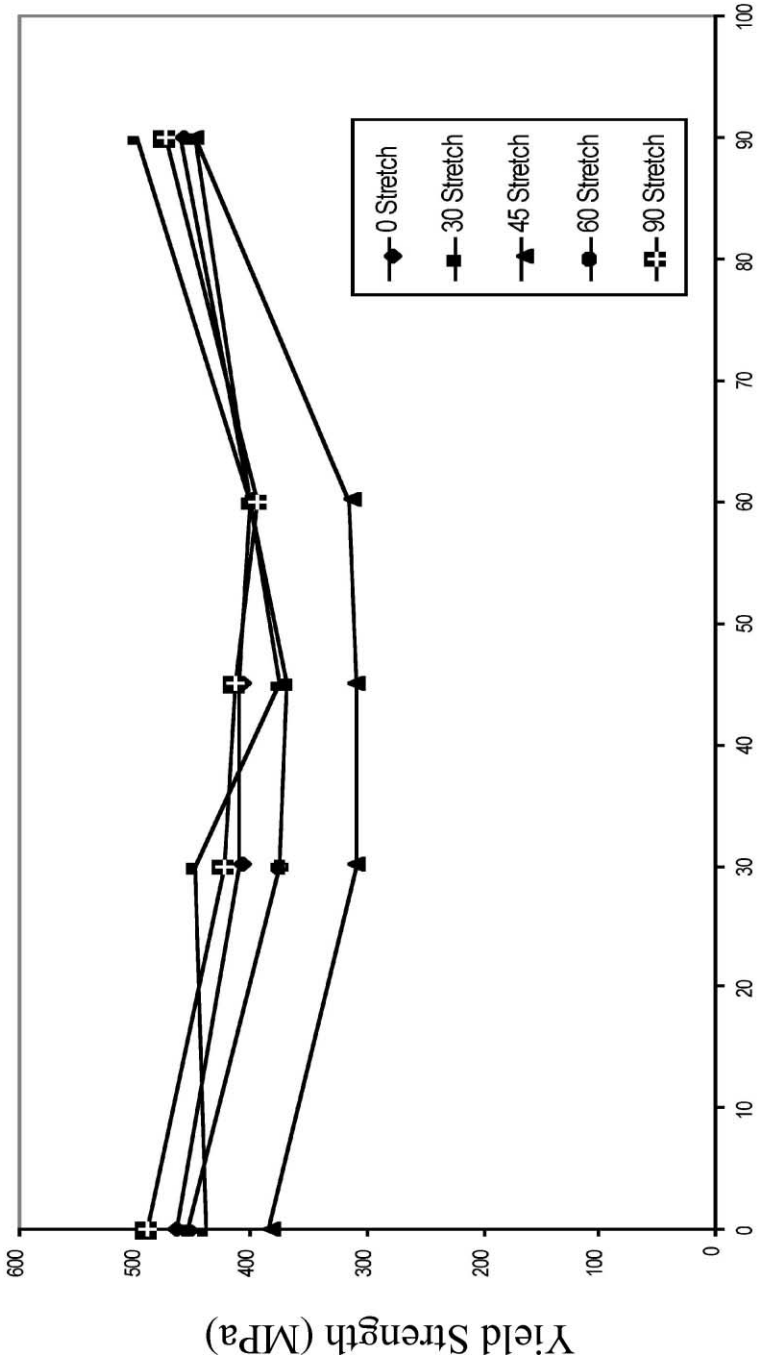

Fig. 1. Measured anisotropy of yield strength in 2090 Al–Li alloy.

It is reasonably well established in crystal plasticity literature that the functional forms of slip hardening laws carry over to the functional forms of the macroscopic strain hardening (Kalidindi et al., 1992). Therefore, for the present investigation, it is suggested to express the macroscopic yield strength of the alloy in forms analogous to Eqs. (7) and (8), as

$$\sigma^{\text{aged}} = M s_o + M' K^{\text{cp}} \bar{\varepsilon} \tag{9}$$

$$\sigma^{\text{aged}} = M s_o + M'' K^{\text{ncp}} \bar{\varepsilon} \tag{10}$$

In Eqs. (9) and (10) the first term denotes the contribution from texture alone, where s_o represents the isotropic contribution from homogenous distribution of precipitates, among other sources. The second term in these equations captures the anisotropic effect of in-homogenous distribution of precipitates. $\bar{\varepsilon}$ in these equations represents the magnitude of the equivalent strain during the cold-work. The factors M' and M are analogous to Taylor factor, but are dependent both on texture as well as the slip activity during the cold-working step prior to the aging step, and their numerical values can be established in a manner that is quite similar to that of evaluating the Taylor factors. For example, for a given texture and a given cold-working process, the values of M and $\bar{\varepsilon}$ are known a priori, the value of K^{cp} can be prescribed arbitrarily, and the yield strength can be predicted using the Taylor-type model described in the previous section [however, unlike in step 1, we now use different values of slip resistances for different slip systems using Eq. (7)]. Then the value of M' can be back-calculated from Eq. (9) using the predicted value of the yield strength. Note that the value of M' obtained by this process is independent of the prescribed value of K^{cp}. A similar technique can be used to evaluate the values of M, by using Eqs. (8) and (10) in place of (7) and (9).

After establishing the values of the parameters M' and M for the specific texture and the cold-working step, plots of $\left(\sigma_y - M' K^{\text{cp}} \bar{\varepsilon}\right)/\mathrm{M}$ and $\left(\sigma_y - \mathrm{M}'' \mathrm{K}^{\text{ncp}} \bar{\varepsilon}\right)/\mathrm{M}$ against the angle to the rolling direction should be made, where σ_y is the measured yield strength. Different values of the parameters K^{cp} and K^{ncp} may be used in multiple plots to establish the trends. According to Eqs. (9) and (10), if the values of $\left(\sigma_y - M' K^{\text{cp}} \bar{\varepsilon}\right)/\mathrm{M}$ or $\left(\sigma_y - \mathrm{M}'' \mathrm{K}^{\text{ncp}} \bar{\varepsilon}\right)/\mathrm{M}$ become independent of the angle to the rolling direction, then it would provide a strong indication in favor of the possible co-planar or non-co-planar slip hardening mechanisms, respectively.

It is suggested that this methodology be applied to a sufficiently large database to identify a consistent trend. Finally, it should be recognized that the methodology presented here provides a simple but powerful tool to understand and establish the physical trends in the experimental data.

3. Application to Al–Li 2090-T8E41

In the present study, it was decided to apply this methodology to understand the yield strength anisotropy in Al–Li 2090-T8E41 alloy sheets. The sheets were processed

as follows. The as-received hot rolled sheets (1.57 mm thickness) were solution heat treated at 510 °C for 30 min. Large samples (6×6 in and 10×12 plates) were then cut from the sheet and given a 6–10% off-axis stretch at 0, 30, 45, 60 and 90° (stretch axis) to the original rolling direction. All the specimens were then aged at 180 °C for 24 h. Tensile coupons were then machined from each of these aged samples at 0, 30, 45, 60 and 90° (tensile axis) to the rolling direction, and then tested to failure. The tensile specimens were tested at a constant cross-head speed of 1.27 mm/min.

The effect of the off-axis stretch on the yield strength anisotropy in the sheet is shown in Fig. 1. A similar behavior was discussed by Lee et al. (1999) for 2095 Al–Cu–Li alloy. The minimum strength was obtained at either 45 or 60° to the rolling direction (RD) in all the sheets produced in this study. The lowest overall strength level was obtained in the samples stretched at 45° to RD. There was significant anisotropy in all sheets produced for this study, which ranged from about 15 to 45%.

Crystallographic texture was measured both in the as-received condition and in the stretched and aged condition. For texture measurements, samples were mechanically polished and etched to remove any residual deformation layers. In all cases, the original rolling direction was used as the pole figure reference direction. The crystallographic texture was measured using the X-ray diffraction technique on a Philips X'Pert PW3040 MRD X-ray diffractometer operating at 40 kV and 50 mA using CuK_α radiation. The diffractometer was equipped with a curve monochromator. Three incomplete pole figures (111), (200), and (220) were obtained using the reflection technique. The resulting data was analyzed using the popLA software package (Kallend et al., 1991) from which the orientation distribution functions (ODFs) were calculated using the spherical harmonic approach.

The initial texture in the as-received material is presented in Fig. 2 as ODF sections. The results are plotted using three Euler angles (φ_1, Φ, φ_2) according to the convention suggested by Bunge (1993). In the as-received state, the material exhibited a very strong Brass component ($\{110\}<112>$) and a weak Copper component ($\{112\}<111>$) with intensities of about 45X and 2X random, respectively. Brass and Copper components occur at locations (φ_1, Φ, φ_2) $=(35, 45, 0)$, $(90, 30, 45)$ respectively. The high Brass intensity is common in Al–Li alloys, especially in the Al–Li superplastic materials. Other significant texture components observed in the as-received material included R $\{124\}<211>$, P $\{110\}<122>$, S $\{123\}<634>$ and shear $\{111\}<112>$ orientations, with intensities of about 9–11X random.

Texture was also measured in the sheets subsequent to the 6–10% off-axis stretch at different angles to the RD and the aging heat treatment described earlier. Some of these are also shown in Fig. 2. Comparison of the textures in Fig. 2, indicates that the texture did not change much during the stretching and aging process. The major change appears to be some weakening (or spreading) of the Brass component.

As described in the previous section, to analyze the experimental data in Fig. 1, we start with the measured texture in the sheet in the as-received condition. The measured texture in the as-received material (Fig. 2) was discretised into 80 weighted grain orientations using popLA (Kallend et al., 1991). There was good correspondence between the pole figures recreated from these weighted grain orientations and the originally measured ones. Starting with the weighted grain orientations repre-

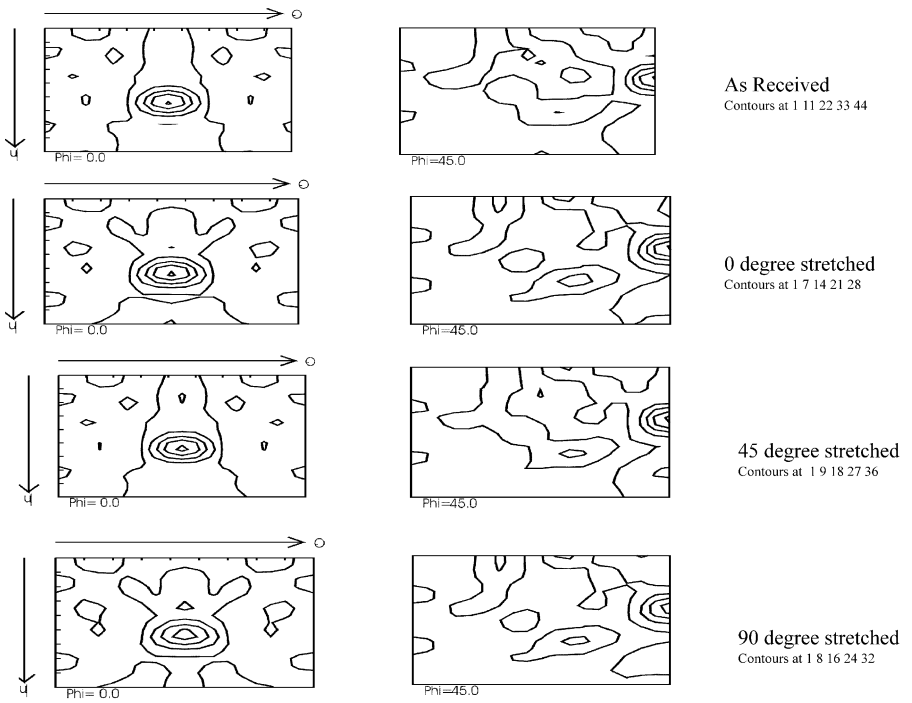

Fig. 2. ODF micrographs of the material at different stages of processing.

senting the initial texture in the as-received sheets, an off-axis stretch of 10% was simulated at 0, 30, 45, 60, and 90° to the rolling direction, using the Taylor-type model described above. In simulating the stretch it was assumed that the material contracts equally in all directions normal to the stretch direction ($R = 1$). The total slip activity on the various slip systems in the 80 grain orientations used in this simulation were tracked. The model also accounts for the small texture changes that occur during the stretch.

Following the procedure outlined in step 1, the Taylor factors were computed for the textures predicted by the Taylor-type model after applying the different off-axis stretches. Fig. 3 depicts the variation of the computed Taylor factors as a function of the angle to the rolling direction for the different sheets. It is observed that the different stretch conditions had only a relatively small effect on the Taylor factors. This is because of the small magnitude of the stretches applied (about 10%), and is quite consistent with the small changes in texture seen in Fig. 2. It is, however quite clear from Fig. 3 that the strong initial texture in the sheets produces a significant variation in the Taylor factor as a function of the angle from the rolling direction, which will in turn produce the same variation in the yield strength of the sheet. In particular, the Taylor factor is observed to change from about 3.5 to about 2.7, which corresponds to about 30% variation in the yield strength. The experimental data

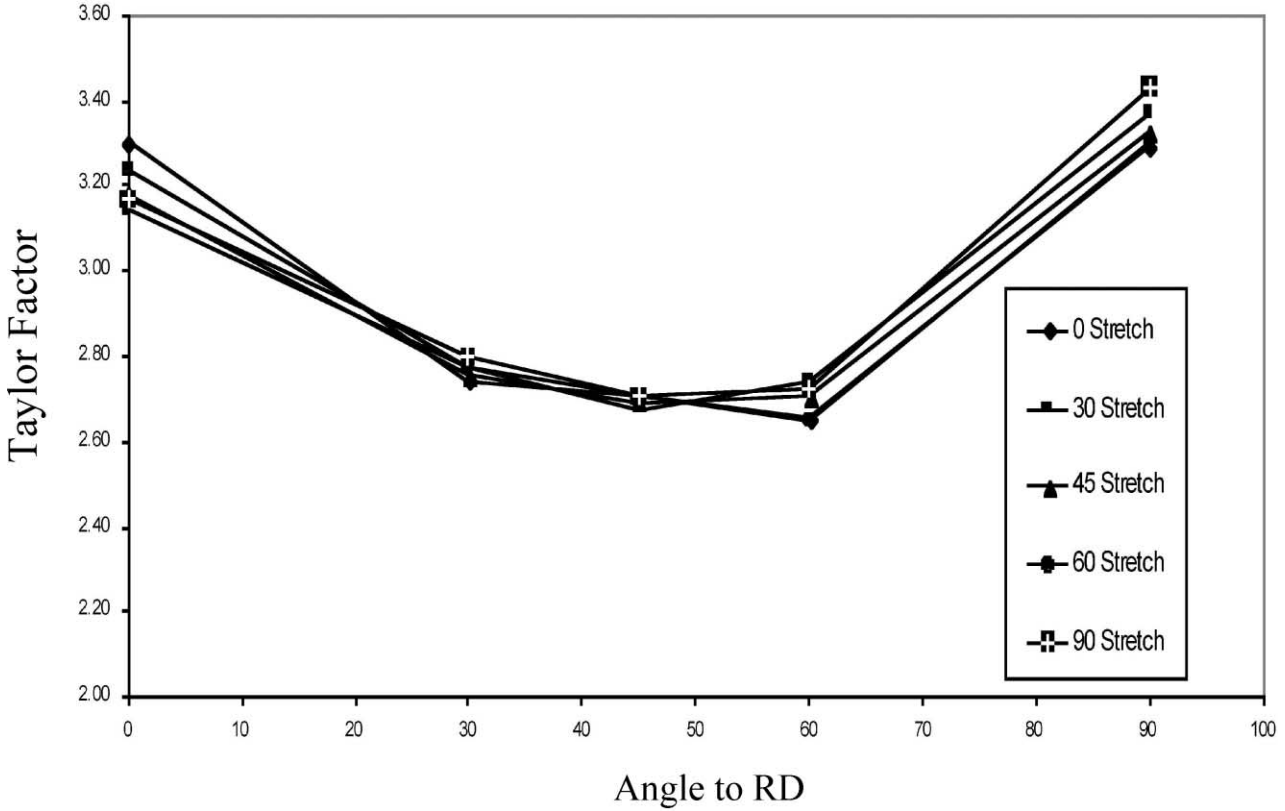

Fig. 3. Variation of the Taylor factor with the angle from the rolling direction for the different stretch conditions.

shown in Fig. 1 was normalized by the Taylor factors (Fig. 3) and plotted in Fig. 4. Fig. 4 indicates that the values of σ_y/M are relatively constant with the angle to the rolling direction, in comparison to Fig. 1. This means that texture does make a substantial contribution to the observed anisotropy in the sheets studied here. There is, of course, significant variation (from a constant value) in these data.

A closer look at the data in Fig. 4 indicates that if the data corresponding to a single stretched condition is isolated and examined, the data exhibits much less scatter about the mean value than the complete data from all the stretched plates. This indicates that there could be significant differences in the average yield strengths of the different plates in the different stretched conditions. Part of this difference, we believe, can be attributed to the fact that the different sheets have not been subjected to the exact same amount of stretching (the applied stretch ranged from 6 to 10% due to experimental difficulties in controlling the stretch value). In order to account for this difference, each curve in Fig. 4 was divided by its average value. These normalized strength factors are plotted in Fig. 5. It is seen that there is much less scatter in Fig. 5 compared to the data in Fig. 4. Once again, it is observed that the yield strength normalized by the Taylor factor is reasonably independent of the angle to the rolling direction, indicating that texture constitutes a major contribution to the observed anisotropy in the sheets studied here.

Next, the contribution to the observed anisotropy from the preferential hardening of slip systems (due to inhomogeneous formation of T_1 precipitates) is investigated following the approach described in step 2 earlier. The values of factors M' and M were computed using the texture at the end of the stretching process and the slip activity during the stretching process, both predicted by the Taylor-type model described earlier. The computed values of M' and M are shown in Figs. 6 and 7 as a function of the angle to the rolling direction in each stretch condition. As anticipated, the values of M' and M are much more sensitive to the stretch condition compared to the Taylor factor M (compare Fig. 3 with Figs. 6 and 7).

After establishing the values of the parameters M' and M, plots of $(\sigma_y - M'K^{cp}\bar{\varepsilon})/M$ and $(\sigma_y - M''K^{ncp}\bar{\varepsilon})/M$ were made with different values of the parameters K^{cp} and K^{ncp}, as suggested in step 2 earlier. Repeated trials with different values of the parameters K^{cp} and K^{ncp} did not produce any better correlations for the *complete set* of the experimental data (Fig. 1) than those already obtained in Fig. 5. This indicates that there is no strong evidence, from a statistical viewpoint, in the present set of data for the operation of any mechanisms leading to significant preferential hardening of slip systems with either co-planar or non-co-planar bias. In our opinion, the contribution to anisotropy from the precipitates in the present set of experiments is of the same order of magnitude as the scatter in the experimental results reported here, and therefore does not allow us to investigate this effect in detail.

We plan to pursue a more extended and rigorous experimental program in the future that will provide more clear evidence. However, we point out that in some cases, we were able to find good correlations with the non-co-planar hardening mechanism [Eq. (8)], when we examined each stretch condition *independently*. As an example, we show in Fig. 8, plots of $(\sigma_y - M''K^{ncp}\bar{\varepsilon})/M$ for the sheet that was stretched at 0 degrees to the rolling direction. In this case, it is clear that a suitable

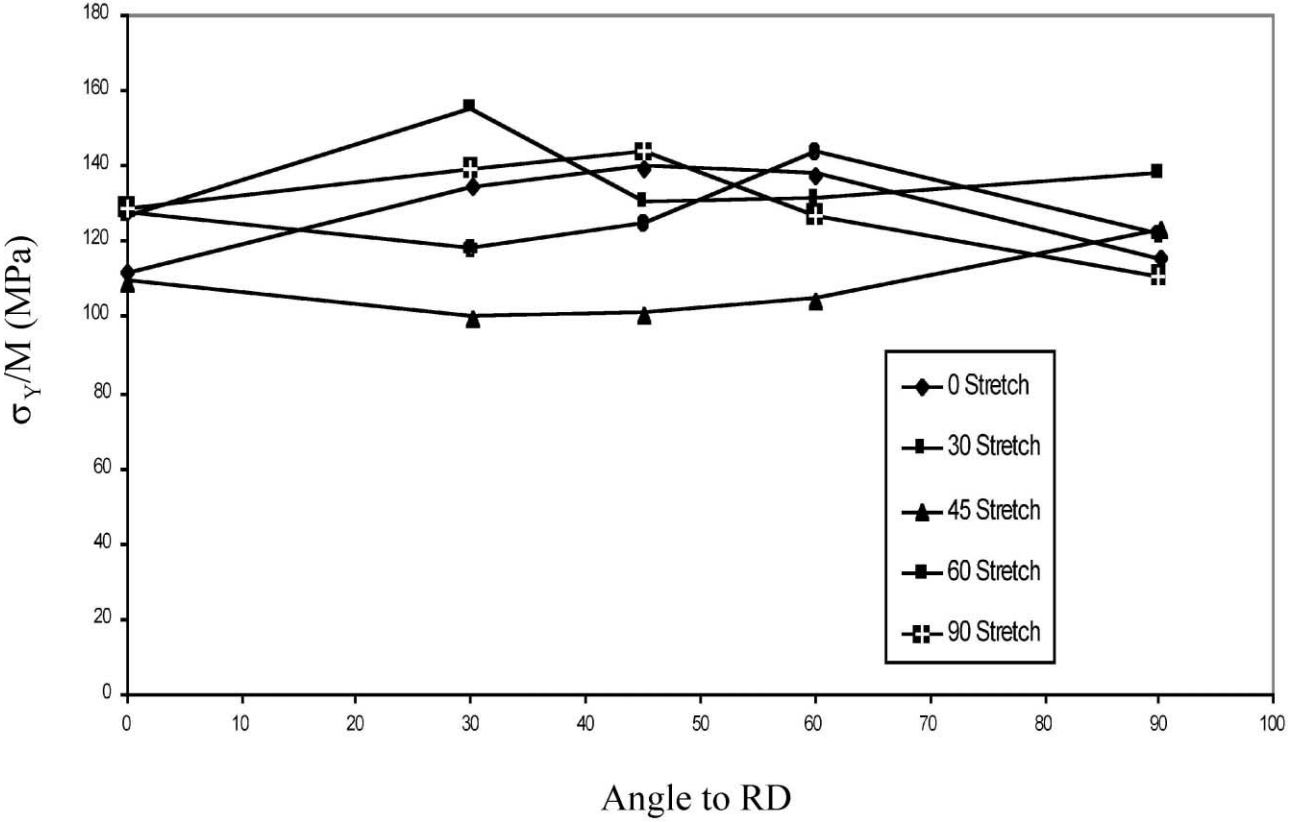

Fig. 4. Measured anisotropy of yield strength in 2090 alloy normalized by Taylor factors.

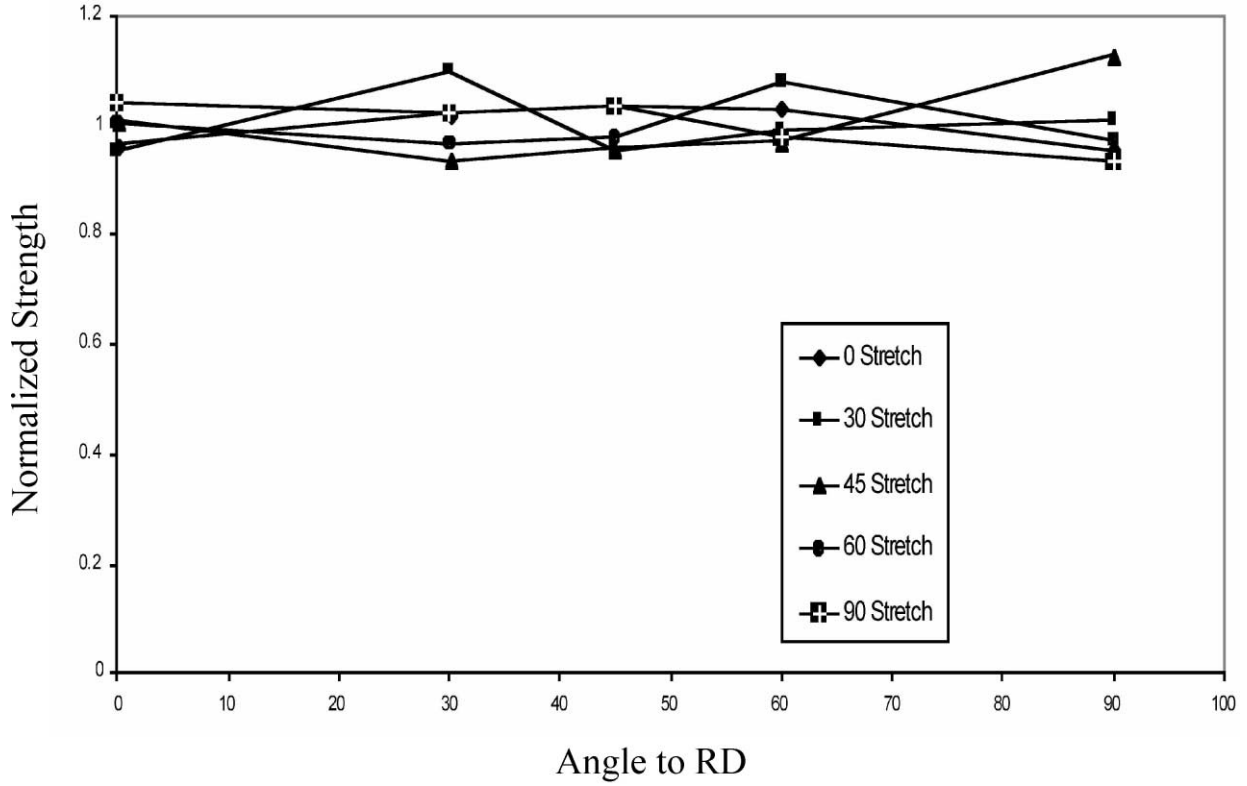

Fig. 5. Measured anisotropy of 2090 alloy normalized by the Taylor factor and divided by the average value of σ_y/M for each stretch condition.

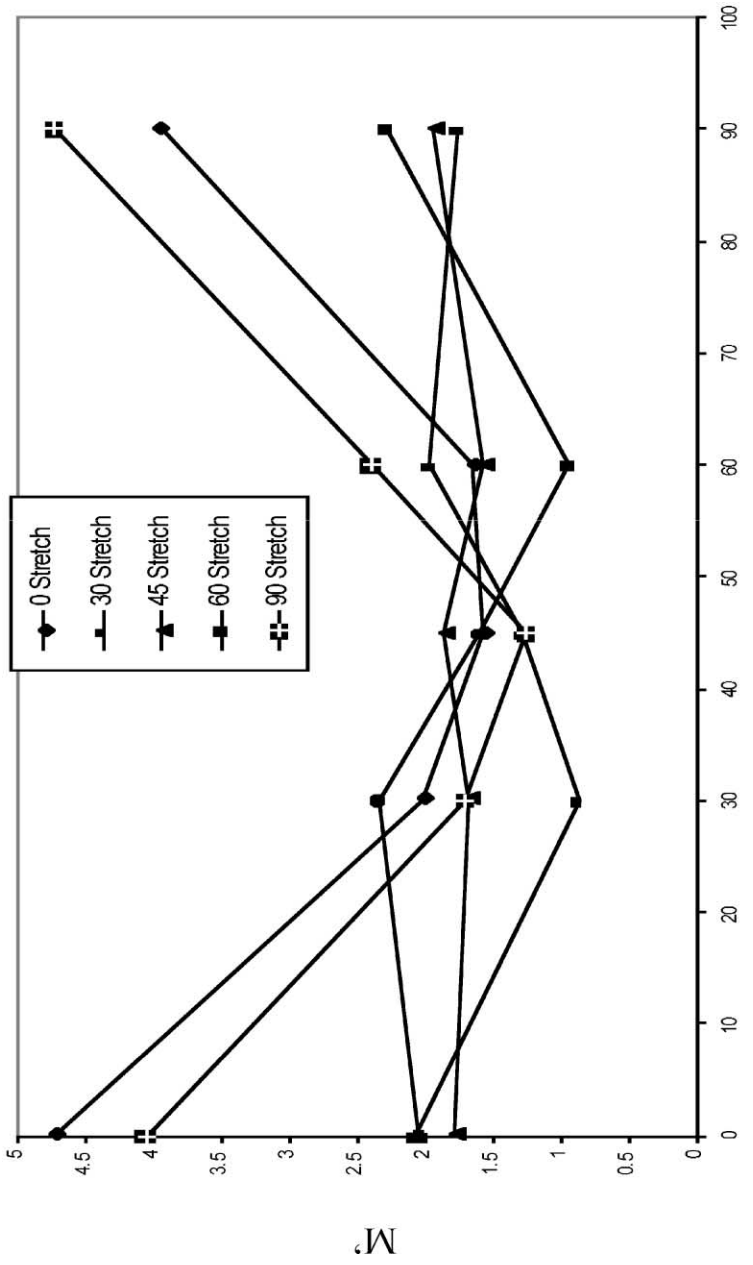

Fig. 6. Influence of co-planar slip hardening on the anisotropy of yield strength.

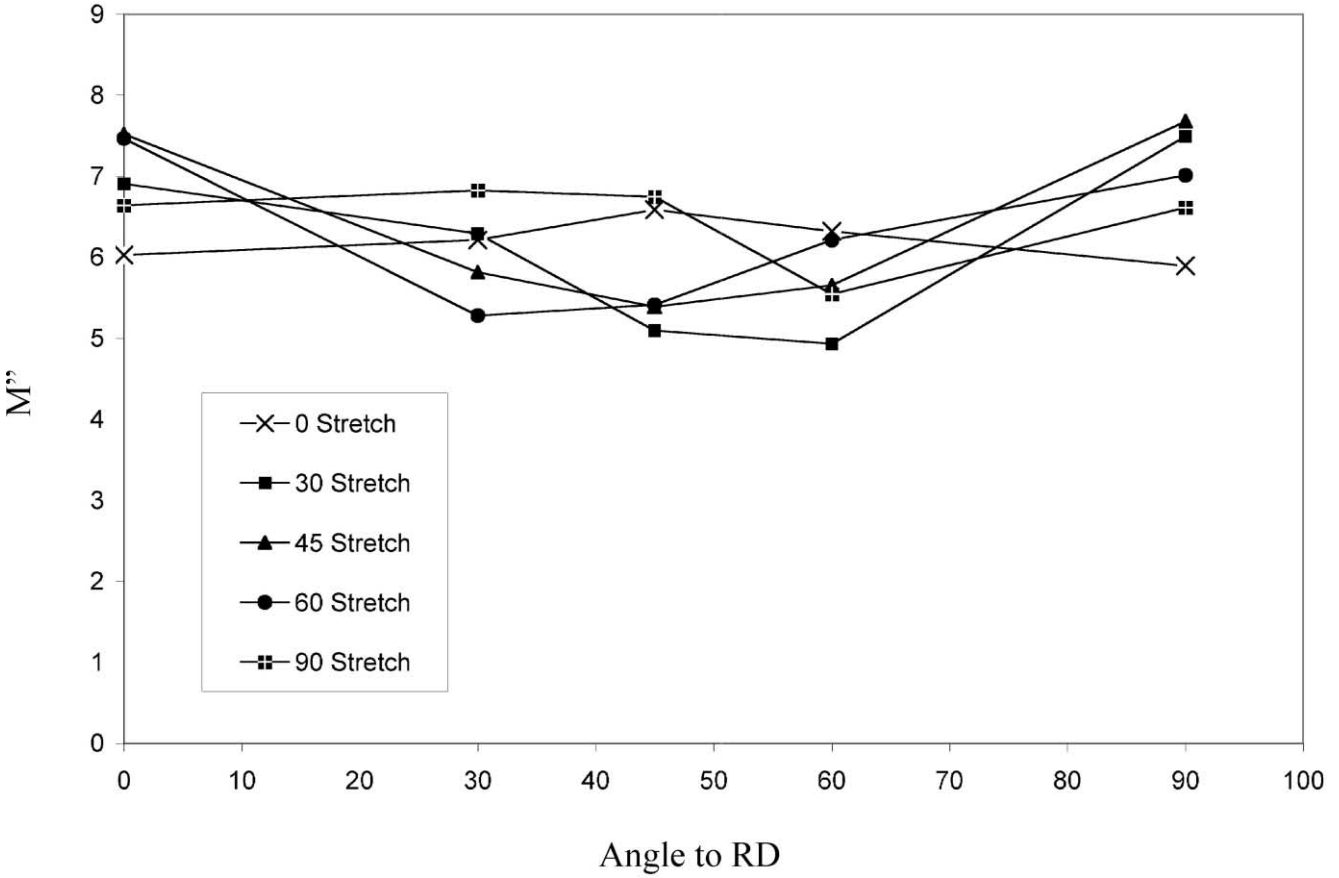

Fig. 7. Influence of non-co-planar slip hardening on the anisotropy of yield strength.

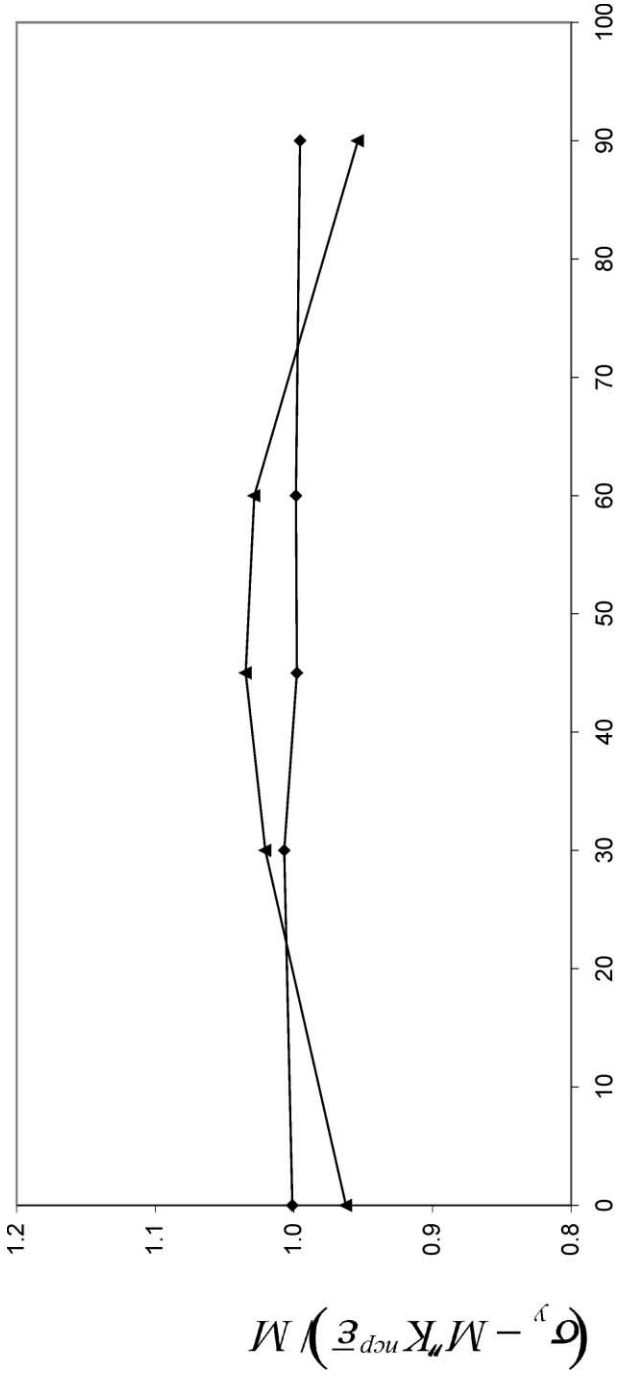

Fig. 8. Role of non-co-planar slip hardening on the the sheet stretched at 0° to the rolling direction.

choice of K^{ncp} produces a good correlation for non-coplanar slip hardening mechanism. That is, with a value of $K^{\mathrm{ncp}} = 180$, we find that $\left(\sigma_{\mathrm{y}} - M'' K^{\mathrm{ncp}} \bar{\varepsilon}\right)/M$ is relatively independent of the angle to the rolling direction, implying that the anisotropy in this sheet can be fully explained by the non-co-planar preferential hardening mechanism during the aging process. Of the five stretch conditions described here, it was found that the non-co-planar hardening model produced a positive correlation with the data presented for three stretch conditions [i.e. the plots $\left(\sigma_{\mathrm{y}} - M'' K^{\mathrm{ncp}} \bar{\varepsilon}\right)/M$ became more independent of the angle to RD]. For the other two stretch conditions, neither of the models produced a positive correlation. This is largely because much of the anisotropy in the present dataset originated by texture. The cold-working and subsequent aging process produced a relatively smaller contribution to the overall anisotropy, perhaps because of the small amounts of cold work used in the present study. In a future experimental program, we plan to apply a larger amount of cold work, which may adversely affect the ductility of the alloy but is likely to produce more clear correlations with the models.

4. Conclusions

A crystal plasticity based modeling framework was presented to allow one to decouple the contributions to the overall anisotropy from crystallographic texture and precipitation hardening, and to correlate the contribution from the latter to either co-planar slip activity or the non-co-planar slip activity in the cold-working step prior to the aging heat treatment. The methodology developed in the study was illustrated on a limited dataset of experiments on Al–Li 2090-T8E41 alloy sheet. The application of the methodology developed in this study revealed that much of the observed anisotropy in this particular data set could be explained by accounting for the texture in the sample in the processed condition. Beyond texture, there appears to be a contribution from precipitation hardening to the overall anisotropy of these alloys. Application of the proposed methodology to the present data set revealed that this contribution, although secondary in the present data set, could be explained as arising from preferential non-coplanar hardening of the slip systems that were active during the off-axis stretch.

Acknowledgements

The authors wish to thank the National High Magnetic Field Laboratory for laboratory facilities. The authors also recognize the support from the School of Computational Sciences and Information Technology. The authors would like to acknowledge the support from the National Science Foundation, Materials Program (DMR 1906-713-32). The authors also acknowledge the support from the Center for Materials Research and Technology (MARTECH) and Center for Nonlinear Non-Equilibrium Phenomena (Cennas). S.K. wishes to acknowledge financial support from NSF—DMR 9612343.

References

Asaro, R.J., Needleman, A., 1985. Texture development and strain hardening in rate dependent polycrystals. Acta Metall. 33, 923–953.

Bronkhorst, C.A., Kalidindi, S.R., Anand, L., 1992. Polycrystalline plasticity and the evolution of crystallographic texture in FCC metals, PhD. Trans. Roy. Soc. Lond. A 341, 443–477.

Barlat, F., Becker, R.C., Hayashida, Y., Maeda, Y., Yanagawa, M., Chung, K., Brem, J.C., Lege, D.J., Matsui, K., Murtha, S.J., Hattori, S., 1997. Yielding description for solution strengthened aluminum alloys. Int. J. Plasticity 13 (4), 385–401.

Bunge, H.J., 1993. Texture Analysis in Materials Science (Peter R. Morris, Trans.). Cuvillier Verlag, Gottingen.

Ceccaldi, D., Yala, F., Baudin, T., Penelle, R., Royer, F., Arminjou, M., 1994. Deformation textures and plastic anisotropy of steels using Taylor and nonhomogeneous models. Int. J. Plasticity 10 (6), 643–662.

Chandler, H.D., Gortzen, J.N., 1994. Kinetics of tensile deformation in a precipitation-hardened aluminum alloy. Materials Science and Engineering A 188, 97–102.

Choi, S.H., Barlat, F. and Liu, J., 2000. Effect of precipitates on the plastic anisotropy of polycrystalline aluminum alloys. Mater. Sci. Forum 331–3: Part 1–3, 1327–1332.

Es-Said, O.S., Lee, E.W., 1995. The effect of stretch orientation (and rolling mode) on the tensile behavior of 2095 aluminum lithium alloy. In: Lee, E.W., Jata, N.V., Frazier, W.E. (Eds.), Light Weight Alloys for Aerospace Applications III. TMS, Las Vegas.

Flower, H.M., Gregson, P.J., 1987. Critical assessment solid state phase transformations in aluminum alloys containing Lithium. Mater. Sci. Technol. Ser. 3 (2), 81–90.

Gall, K., Sehitoglu, H., 1999. The role of texture in tension-compression asymmetry in polycrystalline NiTi. Int. J. Plasticity 15 (1), 69–92.

Garmestani, H., Vaghar, M., Hart, E.W., 2001. A unified model for inelastic deformation of polycrystalline materials—application to transient behavior in cyclic loading and relaxation. Int. J. Plasticity 17 (10), 1367–1391.

Inal, K., Wu, P.D., Neale, K.W., 2000. Simulation of easing in textured aluminum sheets. Int. J. Plasticity 16 (6), 635–648.

Kalidindi, S.R., Schoenfeld, S.E., 2000. On the production of yield surfaces by crystal plasticity models for FCC polycrystals. Mater. Sci. Eng. A293, 120–129.

Kalidindi, S.R., Bronkhorst, C.A., Anand, L., 1992. Crystallographic texture evolution during bulk deformation processing of FCC metals. Journal of the Mechanics and Physics of Solids 40, 537–569.

Kallend, J., Kocks, U.F., Rollett, A.D., Wenk, H.R., 1991. Operational texture analysis. Mater. Sci. Eng. A132, 1–11.

Kaneko, K., Omayaka, T., 2000. A viscoplastic constitutive model with effect of aging. Int. J. Plasticity 16 (3-4), 337–358.

Khan, A.S., Cheng, P., 1998. An anisotropic elastic–plastic constitutive model for single and polycrystalline metal. II—experiments and predictions concerning thin-walled tubular OFHC copper. Int. J. Plasticity 14 (12), 209–226.

Kim, N.J., Lee, E.W., 1993. Effect of T1 precipitate on the anisotropy of Al–Li alloy 2090. Acta Metall. Mater. 41, 941–948.

Kim, J.B., Yang, D.Y., Yoon, J.W., et al., 2000. The effect of plastic anisotropy on compressive Instability in sheet metal forming. Int. J. Plasticity 16 (6), 649–676.

Lee, E.W., Frazier, W.E., 1988. The effect of stretch on the microstructure and mechanical properties of 2090 Al–Li. Scripta Metall. 22, 53–57.

Lee, E.W., Kalu, P.N., Brandao, L., Es-Said, O.S., Foyos, J., Garmestani, H., 1999. The effect of off-axis thermomechanical processing on the mechanical behavior of textured 2095 Al–Li alloy. J. Mater. Sci. Eng. A265, 100–109.

Li, M., Barlat, F., 2000. Metal Forming, special issue. Int. J. Plasticity 16 (6), 593.

Lin, G., Havner, K.S., 1994. On the evolution of texture and yield loci in axisymmetric deformation of f.c.c polycrystals. Int. J. Plasticity 10 (5), 471–498.

Lucke, K., Hirsch, J., Engler, O., Rickert, T., 1986. Rolling and recrystallization textures of Al alloys in

presence of precipitation. In: Starke, J.E.A., Sanders, J.T.H. (Eds.), Aluminum Alloys—Their Physical and Mechanical Properties. EMAS, University of Virginia, Charlottesville, VA.

Miller, W.S., White, J., Lloyd, D.J., 1986. The metallurgy of Al–Li based alloys. In: Starke, E.A., Sanders, J.T.H. (Eds.), Aluminum alloys—Their Physical and Mechanical Properties. EMAS, University of Virginia, Charlottesville, VA.

Peeters, B., Hoferlin, E., Van Houtte, P., Aernoudt, E., 2001. Assessment of crystal plasticity based calculation of the lattice spin of polycrystalline metals for FE implementation. Int. J. Plasticity 17 (6), 819–836.

Peters, M., Welpmann, K., Zink, W., Sanders Jr., T.H., 1986. Fatigue behavior of Al–Li–Cu–Mg alloy. In: Baker, C., Gregson, P.J., Harris, S.J., Peel, C.J. (Eds.), Inst. of Metals, London, England, pp. 239–246.

Taylor, G.I., 1938. Plastic strain in metals. J. Inst. Metals 162, 307.

Trinca, M., Avalino, A., Garmestani, H., Foyos, J., Lee, E.W., Es-Said, O.S., 2000. Effect of rolling orientation on the mechanical properties and crystallographic texture of 2195 aluminum–lithium alloy. Materials Science Forum 331-337, 849–854.

Tsao, C.S., Lin, T.L., Yu, M.S., 1999. A small angle X-ray scattering study of late stage delta precipitation in Al–7.9% Li alloy for growth kinetics and dynamics scaling. Physica B 271 (1-4), 322–331.

Vasudevan, A.K., Fricke, W.G., Malcolm, R.C., 1988. On through thickness crystallographic texture gradient in Al–Li–Cu–Zr alloy. Metall. Trans. 19A, 731.

Yao, D., Chu, D., Morris, J.W., 1991. Tensile deformation of Al–Cu–Li–Zr alloy—2090-T8E4l at 298 and 77 K. In: Lee, E.W., Kim, N.J. (Eds.), Light-Weight Alloys for Aerospace Applications II. TMS, New Orleans.

Yoon, J.W., Barlat, F., Chung, K., et al., 2000. Earing predictions based on asymmetric nonquadratic yield function. Int. J. Plasticity 16 (9), 1075–1104.